

# Modeling and Estimation of Internal Friction in Cloth

Eder Miguel  
URJC Madrid

Rasmus Tamstorf  
Disney Animation Studios

Derek Bradley  
Disney Research Zurich

Sara C. Schwartzman  
URJC Madrid

Bernhard Thomaszewski  
Disney Research Zurich

Bernd Bickel  
Disney Research Zurich

Wojciech Matusik  
MIT CSAIL

Steve Marschner  
Cornell University

Miguel A. Otaduy  
URJC Madrid

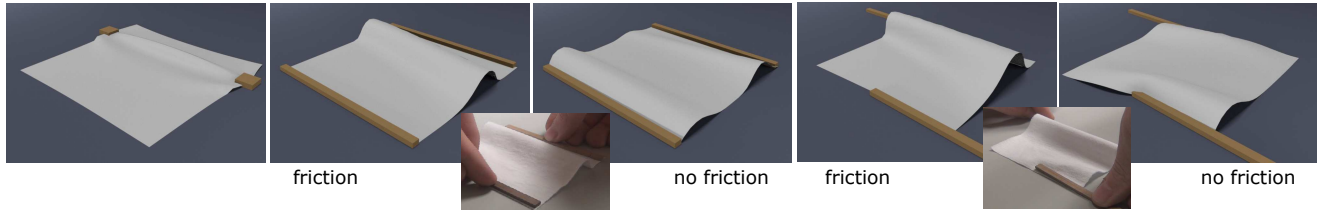


**Figure 1:** We produce a wrinkle on a piece of cotton (first from left). With internal friction (second and fourth), it becomes a ‘preferred wrinkle’ and arises repeatedly under diverse deformations. Without internal friction (third and fifth), folds and wrinkles show no clear similarity. The insets show real-world deformations for the same experiment.

## Abstract

Force-deformation measurements of cloth exhibit significant hysteresis, and many researchers have identified internal friction as the source of this effect. However, it has not been incorporated into computer animation models of cloth. In this paper, we propose a model of internal friction based on an augmented reparameterization of Dahl’s model, and we show that this model provides a good match to several important features of cloth hysteresis even with a minimal set of parameters. We also propose novel parameter estimation procedures that are based on simple and inexpensive setups and need only sparse data, as opposed to the complex hardware and dense data acquisition of previous methods. Finally, we provide an algorithm for the efficient simulation of internal friction, and we demonstrate it on simulation examples that show disparate behavior with and without internal friction.

**CR Categories:** I.3.7 [Computer Graphics]: Three-Dimensional Graphics and Realism—Animation

**Keywords:** cloth simulation, friction, hysteresis

**Links:** [DL](#) [PDF](#)

## 1 Introduction

Clothing is a fundamental aspect of our expressiveness, hence computer animation research has put a lot of effort toward realism and efficiency in cloth simulation [Terzopoulos et al. 1987; Volino et al. 1995; Baraff and Witkin 1998; Bridson et al. 2002]. Computer graphics approaches to cloth simulation build on various types of

elasticity models [Choi and Ko 2002; Eitzmuß et al. 2003; Grinspun et al. 2003; Volino et al. 2009; Thomaszewski et al. 2009], sometimes with the addition of plasticity under large deformations [Bergou et al. 2007]. However, several works in mechanical engineering and computer graphics point out the existence of significant hysteresis between load and unload paths in force-deformation measurements with real cloth, and refer to internal friction, currently missing in computer graphics models, as the phenomenon inducing such hysteresis [Lahey 2002; Ngo-Ngoc and Boivin 2004; Williams 2010].

Ignoring internal friction when estimating elasticity parameters under existing procedures may lead to bias [Volino et al. 2009; Wang et al. 2011; Miguel et al. 2012]. Even if the elastic parameters are chosen to fit the average of loading and unloading behaviors, given observed hysteresis as high as 50% of the average force, ignoring internal friction may induce deformation errors of up to  $\pm 25\%$  for a given load. Internal friction also plays a central role in the formation and dynamics of cloth wrinkles. We have observed that internal friction may induce the formation of ‘preferred’ wrinkles and folds as shown in Fig. 1, persistent deformations as shown in Fig. 14, and history-dependent wrinkles as shown in Fig. 12, and may also make folds and wrinkles settle faster as shown in Fig. 13.

Plasticity models appear to be an alternative way to capture persistent deformations due to large applied loads. However, in their popular form they exhibit no hysteresis under moderate deformations, and they require large reverse loads to eliminate persistent deformations. By contrast, internal friction produces local hysteresis even for small offset deformations, and it requires minor load oscillations to eliminate persistent deformations. These differences make friction more suitable as a source of ‘locally persistent wrinkles’. Plasticity and internal friction are two different phenomena, both of which can occur, and we are studying friction because it is a good explanation of the hysteresis commonly seen in cloth measurements made at moderate strains.

We propose to model internal friction in cloth using Dahl’s model [Dahl 1968]. Others have already identified Dahl’s model as a good match to hysteresis behavior in cloth, including the lack of significant static friction [Lahey 2002; Ngo-Ngoc and Boivin 2004]. However, as we will discuss in Section 3, we also identify features that are not well captured by a standard Dahl model, and propose an augmented reparameterization of the model that includes a strain-dependent definition of hysteresis.

Permission to make digital or hard copies of all or part of this work for personal or classroom use is granted without fee provided that copies are not made or distributed for profit or commercial advantage and that copies bear this notice and the full citation on the first page. Copyrights for components of this work owned by others than the author(s) must be honored. Abstracting with credit is permitted. To copy otherwise, or republish, to post on servers or to redistribute to lists, requires prior specific permission and/or a fee. Request permissions from [Permissions@acm.org](mailto:Permissions@acm.org).  
SA '13, November 19 - 22 2013, Hong Kong, Hong Kong.  
Copyright is held by the owner/author(s). Publication rights licensed to ACM. ACM 978-1-4503-2481-6/13/11\$15.00. <http://dx.doi.org/10.1145/2508363.2508389>

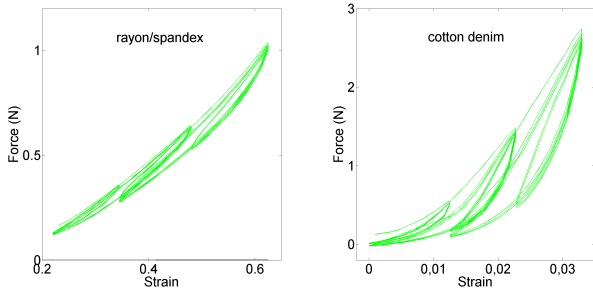


**Figure 2:** Force-deformation curves for load-unload cycles of uni-form stretch on a rayon/spandex knit (left) and denim (right).

We also propose simple and inexpensive data-driven procedures for friction parameter estimation, described in Section 4. In contrast to previous work, which relied on complex force-deformation measurement systems with uniform strain, controlled deformation velocity, and dense data acquisition [Kawabata 1980], our procedures need only sparse data and can deal with non-uniform strain. We demonstrate procedures for stretch and bending acquisition that lead to simple optimization problems for parameter estimation.

In Section 5, we present a simple algorithm for the efficient simulation of internal friction using implicit integration methods. We validate our parameter estimation for several fabrics by simulating the acquisition procedures, and we also show cloth animation examples that exhibit disparate behavior with and without internal friction.

## 2 Background and Related Work

Several works show evidence of hysteresis behavior in tensile deformation experiments with cloth [Breen et al. 1994; Eberhardt et al. 1996; Lahey 2002; Ngo-Ngoc and Boivin 2004]. To illustrate hysteresis, we performed several cycles of uniform stretch deformations on a few samples of different cloth materials using a controlled force-and-deformation capture setup designed after [Miguel et al. 2012]. Fig. 2 shows plots of measured end-to-end distance vs. applied force for 10cm  $\times$  10cm square pieces of rayon/spandex knit (left) and denim (right). We applied loading-unloading cycles between 20% and 60% stretch for rayon/spandex and between 0% and 3% for denim, centered at different offset deformations. We repeated the tests under deformation speeds ranging from 0.5mm/s to 2mm/s, obtaining very similar force values. These experiments relied on complex hardware consisting of electronic actuators, force sensors, and stereo vision capture, with the purpose of capturing high-resolution and accurate data. Our estimation procedures, described in Section 4, rely on very simple setups instead.

We draw the following conclusions from the force-deformation data in Fig. 2. First, hysteresis is a strong effect, with a ratio  $\frac{F_{\max} - F_{\min}}{F_{\text{avg}}}$  at a given deformation of up to 50%. Second, the amount of hysteresis depends on the deformation range of the load-unload cycle and the offset deformation. Third, the transition from the load to un-load path and back exhibits pre-sliding, i.e., the opposing friction grows smoothly, not sharply. In our work, we show that a model of internal friction based on Dahl’s model can replicate this behavior.

Another interesting conclusion about hysteresis is that it produces persistent deformations. Fig. 3-left shows an ideal linear elastic force with ideal hysteresis cycles. In the unload path, the displacement stops when the total internal stress is canceled, producing a persistent deformation  $\epsilon_{\text{per}}$ . We have observed such persistent deformations in stretch and bending experiments with real cloth, and we show that Dahl’s model can replicate this behavior too.

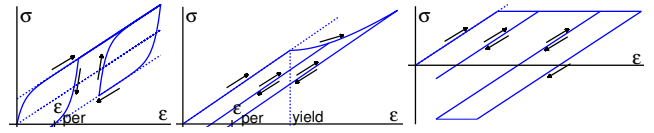


**Figure 3:** Persistent deformations and hysteresis under friction and plasticity models. Left: hysteresis loops added to a linear-elastic model; Center: creep model with plasticity saturation [Müller and Gross 2004]; Right: bounded elasticity model [Bergou et al. 2007].

In the rest of this section we will discuss mechanical effects that affect internal forces, namely, elasticity, plasticity, and internal friction. We omit viscosity in our discussion because the internal forces arising in our experiments are velocity-independent. In the rest of our exposition, a positive internal force will indicate a force that opposes deformation, hence the total force acting on cloth should be evaluated as  $F_{\text{external}} - F_{\text{internal}}$ .

### 2.1 Elasticity

To model cloth elasticity, we use a thin shell model that separates membrane and bending energies. For membrane elasticity, we adopt the St. Venant-Kirchhoff (StVK) model [Ogden 1997], with strain-energy density  $W(\mathbf{E}) = \frac{\lambda}{2} \text{tr}(\mathbf{E})^2 + \mu \text{tr}(\mathbf{E}^2)$ .  $\mathbf{E}$  is the Green-Lagrange strain tensor, and  $\lambda$  and  $\mu$  are the Lamé constants. With a triangle-based discretization, strain is considered constant per triangle, energy density is integrated over the triangle area  $A$ , and membrane force is computed as  $\mathbf{F} = A \nabla W$ . As previously mentioned, the true membrane force would require a sign change, but we use a positive sign to match classic force-deformation plots. Volino et al. [2009] describe the computation of discrete strain, forces, and Jacobians based on triangle vertex positions.

For bending elasticity, we adopt the discrete shells bending model [Grinspun et al. 2003]. Under this model, the discrete strain associated to a deformed edge can be expressed as  $\epsilon = 3 \frac{\theta - \bar{\theta}}{h}$ , where  $\theta$  (resp.  $\bar{\theta}$ ) is the deformed (resp. undeformed) dihedral angle, and  $h$  is the undeformed average height of the incident triangles. Bending forces are computed as  $\mathbf{F} = A \sigma \nabla \epsilon$ , where  $A = \frac{1}{3} e h$  is the area associated to an edge,  $e$  the rest length of the edge,  $\sigma = k \epsilon$  the bending stress, and  $k$  the bending stiffness.

For our exposition, it is convenient to employ a unified representation of scalar strain and stress components. In the remaining, we denote by  $\epsilon$  (resp.  $\sigma$ ) an arbitrary scalar strain (resp. stress), either the bending strain (resp. stress) or an individual component of the membrane strain (resp. stress). Then we express the force due to a scalar stress on a deformed element with area  $A$  as  $\mathbf{F} = A \sigma \nabla \epsilon$ , with  $\sigma = k \epsilon$ , and  $k$  the stiffness of the stress on the element.

There has been extensive work on the estimation of strain-dependent elastic parameters from force-deformation measurements [Eitzmuß et al. 2003; Volino et al. 2009; Wang et al. 2011; Miguel et al. 2012]. The Kawabata Evaluation System (KES) [Kawabata 1980] measures stretch, shear, and bending; other procedures such as the Picture Frame test [Culpin 1979] or the Cantilever test [Clapp et al. 1990] target specific deformation modes; and some recent approaches incorporate computer vision to acquire non-uniform deformations [Miguel et al. 2012]. The work of Wang et al. [2011] is particularly interesting due to the high estimation quality combined with simple acquisition procedures.

### 2.2 Plasticity

As shown in Fig. 3-left, one of the effects of hysteresis is the existence of persistent deformations. It is therefore reasonable to con-

sider plasticity models as an option to model hysteresis. Indeed, Kim et al. [2011] designed a complex model of plasticity with ten parameters to produce persistent cloth wrinkles. Their model modifies the stiffness and rest angle of a bending spring when its strain rate exceeds a threshold value. The recent work of Narain et al. [2013] focuses on resolving the geometric detail in folded and crumpled sheets under plastic deformation.

Common plasticity models separate elastic strain (which defines elastic energy) from plastic strain (which does not change elastic energy). Two common models are a creep model that saturates to a maximum plastic strain [Müller and Gross 2004] and a bounded elasticity model [Bergou et al. 2007], as shown in Fig. 3-center and Fig. 3-right respectively. The curves evidence that plasticity models are not a good match for the hysteresis observed in cloth. A plastic material deforms elastically until the material’s yield strength is exceeded, then abruptly gives way and begins deforming irreversibly. By contrast, hysteresis is prominent in cloth even for small deformations, and its effects increase gradually as deformation is increased. Moreover, even in the plastic regime, the response of plasticity models to reversed loads is purely elastic, whereas cloth exhibits local hysteresis. Another important difference between plasticity and hysteresis is that persistent plastic deformations require a large reverse load to be undone, whereas persistent deformations due to hysteresis can be undone simply by applying small loads that produce narrow hysteresis. We have validated this behavior on stretch experiments with cotton, and it is further discussed in the context of the combination of friction and damping in Section 6.

In this discussion, we did not consider material hardening, but it would not eliminate the fundamental differences. Our model could be complemented with plasticity to capture irreversible wrinkles due to extreme deformations, but based on all previous observations we have discarded plasticity for modeling hysteresis in cloth.

### 2.3 Internal Friction

In cloth, internal friction captures small-scale resistance to inter-yarn motion. When cloth transitions from loading to unloading or vice versa, yarns realign and produce a force that acts against their relative motion. Unlike elastic forces, which oppose deformation (i.e., strain), friction forces tend to act against the change in deformation (i.e., strain rate). Friction and hysteresis have been long studied in mechanical engineering, and there is a large variety of available models. Padthe et al. [2008] survey several models, discuss their mathematical foundations, and analyze their effects.

Probably the most popular friction model is Coulomb’s model. It states that dissipation should be maximized (i.e., strain rate should be minimized), subject to some constraint on the friction stress. For object-object contact, the constraint is posed as a relationship between tangential and normal forces [Baraff 1991]. Coulomb’s model is also generalized to 3D, e.g., for the simulation of granular materials [Zhu and Bridson 2005], by posing constraints on a 3D friction stress tensor. Coulomb’s model succeeds in capturing hysteresis effects, but it may undergo an instantaneous switch of force directions, not present in the data observed on real cloth. Sherburn [2007] simulated cloth at the yarn level using Coulomb’s model for inter-yarn frictional contact. Later, Kaldor et al. [2008] modeled inter-yarn frictional contact combining damping and velocity filters. Recently, Chen et al. [2013] have modeled and estimated friction effects between cloth and other deformable objects.

The works of Lahey [2002] and Ngo-Ngoc and Boivin [2004] constitute the most thorough efforts to model cloth hysteresis using internal friction together with thin shell models. They both captured force-deformation data using KES, and then estimated (strain-independent) parameters of standard friction models. They con-

sidered a second-order Bliman-Sorine model [Bliman and Sorine 1991], which can capture hysteresis, pre-sliding, and the Stribeck effect, i.e., a slight decrease in friction at the transition from static to dynamic regime. However, in their data they found only very subtle Stribeck effects, without which a first-order Bliman-Sorine model, equivalent to a simple Dahl model [Dahl 1968] is sufficient.

We have not observed significant static (internal) friction either, and Dahl’s model, discussed in detail in the next section, produces a good fit to our measured force-deformation data. However, we have found that a strain-independent parameterization fails to capture the strain-dependent magnitude of hysteresis, which is present in our data. This observation also has an impact on the right choice of parameters for model estimation.

Like Lahey [2002] and Ngo-Ngoc and Boivin [2004], we fit a friction model to deformation data. The KES data used in those papers provides dense sampling under uniform strain conditions, whereas our methods work with sparse sampling and non-uniform strain, enabling simpler setups. Furthermore, prior work on internal friction for cloth is limited to the estimation of parameters that fit hysteresis cycles well, but did not analyze the impact on animations.

## 3 Dahl’s Friction Model

In this section we discuss the connection between Dahl’s model and the observed features of hysteresis. Most importantly, we highlight features that are not captured by the standard Dahl model, and propose an augmented reparameterization that is well suited for parameter estimation given force-deformation measurements.

### 3.1 Model and Interpretation

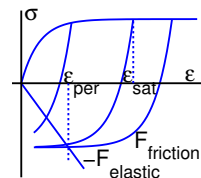
For any scalar strain metric  $\epsilon$  (e.g., weft or warp stretch, shear, or discrete-shells bending strain), Dahl’s model [Dahl 1968] can be used to define a scalar friction stress  $\sigma$  in terms of the change of stress as a function of strain, as follows:

$$\frac{d\sigma}{d\epsilon} = \alpha \left( 1 - s \frac{\sigma}{\sigma_{\max}} \right)^\gamma. \quad (1)$$

$\sigma_{\max}$  is the maximum friction stress,  $\alpha$  is the slope of the stress ratio  $\frac{\sigma}{\sigma_{\max}}$  at  $\sigma = 0$ , and  $s = \text{sign}(\dot{\epsilon})$  indicates the sign of the rate of deformation. In the rest of the paper, we restrict the discussion to a Dahl model with  $\gamma = 1$ . With constant parameters  $\sigma_{\max}$  and  $\alpha$ , this model corresponds to a first-order system with time constant  $\tau = \frac{\sigma_{\max}}{\alpha}$ , and limiting stress  $\sigma_{\max}$  when strain is increasing, or  $-\sigma_{\max}$  when strain is decreasing. Recall that stress is transformed to forces through multiplication by the element’s area  $A$  and the strain gradient  $\nabla\epsilon$ , as discussed in Section 2.1.

To interpret the parameters of Dahl’s model, it is convenient to analyze the behavior of a linear elastic material with friction in the absence of external forces.

The inset shows friction forces under three possible unload paths, as well as (negative) elastic forces. In the loading path, friction adds to the elastic force and saturates in all three cases. In the unloading path, friction gradually decreases and eventually changes sign and opposes elastic forces until an equilibrium is reached. With constant maximum stress,  $\sigma_{\max}$ , the persistent deformation for a linear elastic material with stiffness  $k$  saturates at a value  $\epsilon_{\text{per}} = \frac{\sigma_{\max}}{k}$ . Then, an effective way to tune the maximum friction stress is to specify a desired (maximum) persistent deformation,  $\epsilon_{\text{per}}$ , and the maximum stress is set as  $\sigma_{\max} = k \epsilon_{\text{per}}$ .



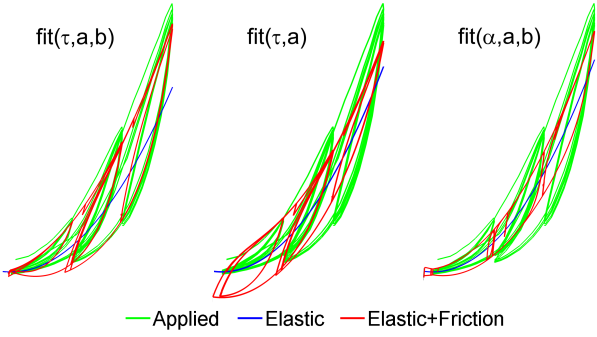


**Figure 4:** Fits of Dahl’s model to the data in Fig. 2-right using as parameterizations: (left) linear  $\sigma_{\max}$  and constant  $\tau$ ; (center) constant  $\sigma_{\max}$  and constant  $\tau$ ; (right) linear  $\sigma_{\max}$  and constant  $\alpha$ .

The unload paths do not reach saturation in all cases though, only when the deformation in the loading path reaches a saturation deformation  $\epsilon_{\text{sat}}$ . For practical reasons, we consider that Dahl’s friction has saturated if it reaches a value  $\|\sigma\| \geq c \sigma_{\max}$  (with, e.g.,  $c = 0.95$ ). Then, based on the analytic solution of first-order systems, the saturation deformation can be computed as  $\epsilon_{\text{sat}} = \epsilon_{\text{per}} + \frac{\sigma_{\max}}{\alpha} \ln \frac{2}{1-c}$ . In other words, an effective way to tune the friction saturation rate is to specify the saturation deformation,  $\epsilon_{\text{sat}}$ , and then the friction saturation rate is automatically set as  $\alpha = \frac{\sigma_{\max}}{\epsilon_{\text{sat}} - \epsilon_{\text{per}}} \ln \frac{2}{1-c}$ .

### 3.2 Parameters for Estimation

The force-deformation data from Fig. 2 suggests that the magnitude of hysteresis grows as the deformation grows. A possible explanation for this growth is that higher strain produces higher inter-yarn normal forces, and hence higher inter-yarn friction. This effect may be captured by a strain-dependent maximum stress  $\sigma_{\max}(\epsilon)$ . Indeed, as shown in Fig. 4, we found that a maximum stress linear w.r.t. strain, i.e.,  $\sigma_{\max} = a + b\epsilon$ , rendered an excellent match to the observed hysteresis data.

With linear maximum stress  $\sigma_{\max}$  and constant slope of the stress ratio  $\alpha$ , the time constant  $\tau$  of Dahl’s model becomes strain-dependent. As shown in Fig. 4, a constant  $\alpha$  does not capture well the profile of hysteresis across the range of deformations in the measured data, while a constant  $\tau$  produces an excellent match.

With these two conclusions in mind, we generalize and reparameterize Dahl’s model as follows:

$$\frac{d\sigma}{d\epsilon} = \frac{\sigma_{\max}(\epsilon) - s\sigma}{\tau}, \quad \text{with } \sigma_{\max}(\epsilon) = a + b\epsilon. \quad (2)$$

For the purpose of parameter estimation, given initial conditions  $\epsilon_0$  and  $\sigma_0$ , the analytic solution can be approximated as

$$\sigma(\epsilon) = s\sigma_{\max}(\epsilon) + (\sigma_0 - s\sigma_{\max}(\epsilon_0))e^{-s\frac{\epsilon - \epsilon_0}{\tau}}. \quad (3)$$

For constant maximum stress, the solution is accurate. For linear maximum stress, it omits a varying offset term bounded by  $\|b\tau\|$ . In practice, we found this term to be small, as well as a source of local minima for parameter optimization; therefore, we resorted to the approximate analytic solution for parameter estimation.

## 4 Estimation of Friction Parameters

Based on the understanding of Dahl’s friction model, in this section we propose simple procedures to estimate its parameters for

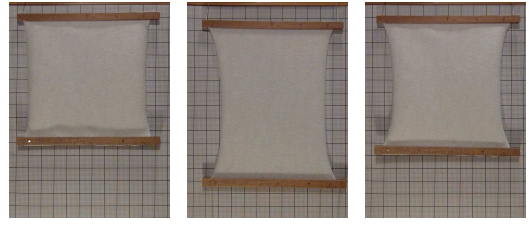


**Figure 5:** Acquisition of stretch for a piece of cotton. From left to right: at rest, deformed under a weight of 6N, and with a persistent deformation back at rest.

different cloth deformation modes. Our procedures each include an acquisition step and a numerical optimization step. By defining simple principles for the acquisition step, we can leverage the analytic definition of friction forces, and thus largely simplify the optimization step. The friction model and the capture principles are general, and we demonstrate them by designing estimation procedures for stretch and bending friction. In both cases, the hardware used for acquisition is extremely simple.

### 4.1 General Rationale

Our parameter estimation procedures share the high-level strategy of many previous approaches for estimating elasticity parameters, namely: apply known position or force boundary conditions, measure the resulting static deformation, and estimate parameters that minimize force and/or position errors for the given conditions. Model estimation is cast as an optimization problem with friction parameters (and possibly elastic parameters) as unknowns.

Elastic forces are defined as explicit functions of elasticity parameters and deformations; therefore, it is straightforward to define an objective function based on force errors, and use optimization methods such as Newton’s or its multiple extensions, which make use of force gradients w.r.t. the parameters. Dahl’s friction forces from Eq. (2), however, are defined in differential form and the derivative is discontinuous. Friction forces are not simply a function of parameters and deformations. They depend on the path followed by those deformations; therefore, the application of Newton-type optimization methods is not straightforward. A possible solution would be to apply slow deformations to the captured material, sample forces and positions densely along the path of deformation, and locally linearize the friction force at each sample.

We propose instead friction estimation procedures that rely on simple capture setups and sparse data. We apply *anchor deformations* where friction forces are saturated, and then reverse the deformation gradually along a monotonic path. Friction forces depend on the path taken, not its duration; therefore, the friction forces at any position along a monotonic path starting at an anchor deformation are defined solely by the current deformation and the anchor deformation. Following this rationale, we can define friction forces as explicit functions of friction parameters and deformations, using the analytic expression in Eq. (3), with the strain and stress at an anchor deformation as initial conditions:  $\epsilon_0 = \epsilon_{\text{anchor}}$ ,  $\sigma_0 = \sigma_{\text{anchor}} = \pm\sigma_{\max}(\epsilon_{\text{anchor}})$ . Then it is straightforward to compute gradients of friction forces and apply Newton-type optimization methods.

With linear maximum stress  $\sigma_{\max}$ , the approximate expression of friction stress Eq. (3) corresponding to a measured deformation with strain  $\epsilon_i$ , anchor deformation  $\epsilon_{\text{anchor},i}$ , and strain-rate sign  $s_i \in \{1, -1\}$  can be rewritten as

$$\sigma_i = s_i(a + b\epsilon_i) - 2s_i(a + b\epsilon_{\text{anchor},i})e^{-s_i\frac{\epsilon_i - \epsilon_{\text{anchor},i}}{\tau}}. \quad (4)$$

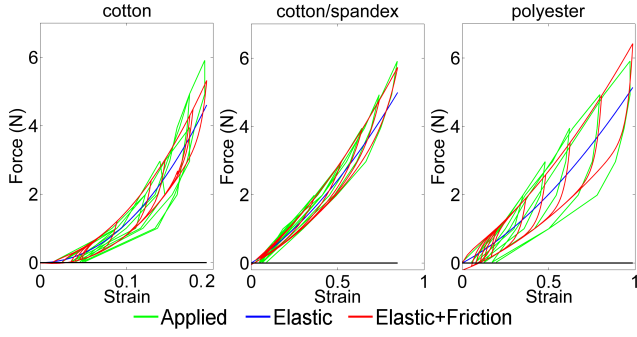


**Figure 6:** Fitting of stretch friction parameters for cloth samples of cotton (left), cotton/spandex (center), and polyester (right).

For practical purposes, in the expression above we assume that strain does not switch signs in the range  $[\epsilon_{\text{anchor},i}, \epsilon_i]$ . For stretch, we perform only tensile experiments, hence the assumption is trivially satisfied. For bending, we suggest performing separate experiments with positive and negative curvatures, and estimating separate parameters in each case.

## 4.2 Estimation of Stretch Friction

To estimate parameters of stretch friction (independently for warp and weft directions), we have devised a procedure to capture force-deformation pairs under quasi-uniform stretch. We place a  $10\text{cm} \times 10\text{cm}$  cloth sample on a vertical plane and we hang various weights from the lower side as shown in Fig. 5. We perform incremental loading and unloading cycles, measuring deformations for weights  $[0, 1, \dots, n, \dots, 1, 0]\text{N}$ , and  $n$  varying from 1 to 6 in our experiments. We repeat the full deformation sequence three times. For each measurement on a loading (resp. unloading) path, we define as anchor deformation the last measurement with a weight of  $0\text{N}$  (resp.  $n\text{N}$ ).

For the  $i^{\text{th}}$  force-deformation measurement, we define a force error as the deviation from force equilibrium between the weight  $F_i$  (which includes the external weight, the clip, and the cloth itself), the elastic force  $k \epsilon_i A \nabla \epsilon_i$ , and the friction force  $\sigma_i A \nabla \epsilon_i$ , i.e.,

$$f_i = F_i - k \epsilon_i A \nabla \epsilon_i - \sigma_i A \nabla \epsilon_i. \quad (5)$$

$k$  is the elastic stiffness,  $A = L_0^2$  is the area of the undeformed cloth of width and length  $L_0$ , and the friction stress  $\sigma_i$  is defined as in Eq. (4) based on the current and anchor strains. We use the Green-Lagrange strain  $\epsilon = \frac{1}{2} \left( \left( \frac{L}{L_0} \right)^2 - 1 \right)$ , where  $L$  is the current length of the cloth. The strain gradient can be computed as  $\nabla \epsilon = \frac{L}{L_0^2}$ .

Given all the force-deformation measurements, we jointly estimate elastic and friction parameters by solving the following least-squares problem:

$$(k, \tau, a, b) = \arg \min \sum_i f_i^2. \quad (6)$$

In our examples, in addition to linear maximum friction stress  $\sigma_{\text{max}} = a + b \epsilon$ , we have also estimated a linear stiffness  $k$ . We have solved the non-linear optimization in Matlab using its built-in trust-region reflective algorithms. To avoid local minima, we initialize the parameters in the following way: first, we fit the stiffness  $k$  with no internal friction, then we fit  $\sigma_{\text{max}}$  with very low  $\tau$  (which approximates Eq. (4) to  $\sigma_i = s_i(a + b \epsilon_i)$ ), and then we fit  $\tau$ .

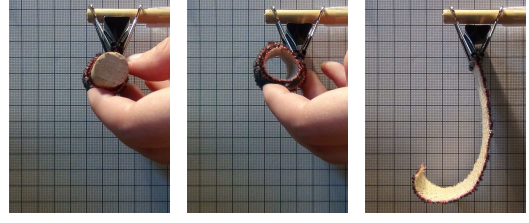


**Figure 7:** Acquisition of bending for a strip of doublecloth. From left to right: rolled around a cylinder, after removing the cylinder, and final spiral shape after unrolling.

**Results and Discussion** We have tested our stretch friction estimation procedure on cloth samples of cotton, cotton/spandex, and polyester. As a reference for the fitting results, the following table shows density ( $\rho$ , in  $\text{kg}/\text{m}^2$ ), stiffness ( $k_1 + k_2 \epsilon$ , in  $\text{N}/\text{m}$ ), maximum friction stress ( $a + b \epsilon$ , in  $\text{N}/\text{m}$ ), and time constant ( $\tau$ , dimensionless) for the warp direction on the three samples.

	$\rho$	$k_1$	$k_2$	$a$	$b$	$\tau$
cotton	0.143	135.6	64.03	2.22	3.16	0.006
spandex	0.157	4.42	32.19	0.40	4.84	0.088
polyester	0.121	26.62	3.64	2.10	5.41	0.031

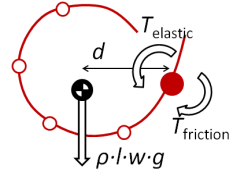
Fig. 6 compares the measured force-deformation data and the results of our parameter estimation for the three materials. The accompanying video shows simulations that resemble the capture procedures and evidence clear differences in the unloading behavior across the three materials.

Thanks to the use of sparse data, our parameter estimation procedures work well with coarser capture resolution, and hence allow the use of less expensive hardware. For compliant cloth such as the one in the examples, inexpensive desktop hardware turns out to be sufficient. For stiffer cloth our desktop setup is not sufficient, but our estimation procedures could reduce the cost of instrumented capture setups and broaden the range of measurable materials.

## 4.3 Estimation of Bending Friction

The key aspect of our procedure to estimate parameters of bending friction is a simple way to produce anchor deformations with controlled strain. We roll a  $10\text{cm} \times 2.5\text{cm}$  strip of cloth around a cylinder of known radius as shown in Fig. 7, and then we gradually unroll the cloth. We have used cylinders with radii of  $[3, 4, 5, 6, 7, 7.5, 10, 16, 23, 27.5, 31.5, 50]\text{mm}$ , and we have repeated the experiment with each cylinder three times. Before each rolling operation, we flatten the strip of cloth to remove possible persistent deformations.

For each experiment, we fit a cubic spline to the profile of the spiral, and we sample it at  $n$  points ( $n = 5$  in our experiments), as shown in the inset. For each of these samples, we define a torque error as the deviation from equilibrium between the gravity torque produced by the cloth's weight, the elastic bending torque, and the bending friction torque. With our simple procedure, the anchor deformation for all  $n$  samples in the same experiment is given by the same initial rolling radius. Next, we will define the elastic, friction, and gravity torques in detail.



The deformed cloth can be regarded as a ruled surface obtained by

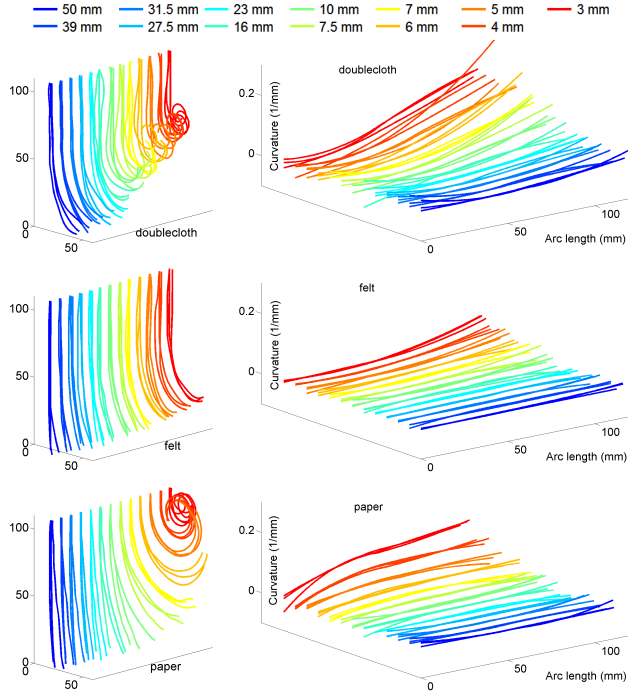


**Figure 8:** Left: Spiral profiles for bending estimation; Right: Curvatures along the spiral profiles. The plots show data for 12 different initial radii and 3 samples per radius. The materials are, from top to bottom, synthetic doublecloth, felt, and paper.

sweeping the spiral profile along the width of the cloth  $w$ . For the derivation of the elastic torque, we assume an infinitely fine regular triangulation with triangles of height  $dh$ . At each sample, we assume a hinge formed by edges of the triangulation running across the width of the cloth. Following the discrete-shells bending model described in Section 2.1, the strain of each edge is  $\epsilon = 3 \frac{d\theta}{dh} = 3 \kappa$ , where  $\kappa$  is the curvature of the spiral profile at the sample. The elastic torque can then be computed as  $T_{\text{elastic}} = k \epsilon dA \nabla_{\theta} \epsilon = 3 k w \kappa$ . The friction torque is defined as  $T_{\text{friction}} = \sigma dA \nabla_{\theta} \epsilon = \sigma w$ , where  $\sigma$  is defined as in Eq. (4) based on the current and anchor strains. Finally, the gravity torque can be computed based on the density of the cloth  $\rho$  as  $T_{\text{gravity}} = \rho l w g d$ , where  $l$  is the length of the hanging piece of cloth, and  $d$  is the horizontal distance from its center of mass to the sample point on the spline.

We can now express a torque error for each spline sample as the deviation from equilibrium,  $T_{\text{gravity}} - T_{\text{elastic}} - T_{\text{friction}}$ . Substituting the expressions defined above, and factoring out the cloth width  $w$ , we obtain an expression of bending stress error for each sample,

$$f_i = \rho l_i d_i g - 3 k \kappa_i - \sigma_i. \quad (7)$$

Note that the final expression is independent of the triangulation.

Same as for the estimation of stretch friction parameters, we formulate a least-squares problem with the form of Eq. (6). However, we use a cantilever experiment [Clapp et al. 1990] to estimate stiffness parameters, because in the spiral shapes of light materials the contribution of gravity is small, and there is not sufficient data to jointly estimate elasticity and friction parameters. To increase the optimization robustness, we first fit  $\sigma_{\text{max}}$  with very low  $\tau$ , and then  $\tau$ , before fitting both together. In addition, we remove sample points where gravity and elastic torques oppose each other, as they do not guarantee a monotonic deformation.

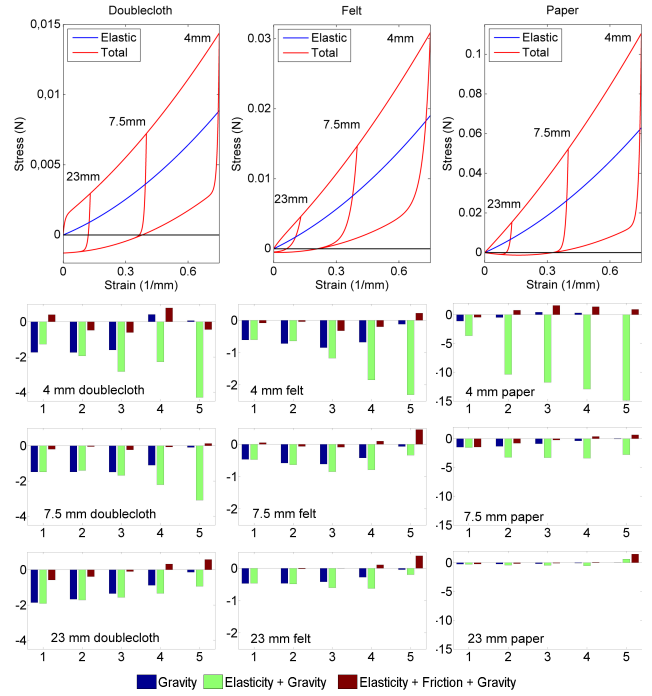


**Figure 9:** Results and validation of bending friction estimation on doublecloth (left), felt (middle), and paper (right). Top row: Estimated hysteresis curves with unload paths for three initial radii (4mm, 7.5mm, and 23mm). Bottom 3 rows: Stress error residuals evaluated at samples on the spiral profiles (shown in Fig. 10). The error in total stress is compared to the gravity and elastic stress.

**Results and Discussion** We have tested our bending friction estimation procedure on materials with a moderately large bending-stiffness-to-density ratio. In particular, we report results for two cloth fabrics, felt and a synthetic doublecloth, as well as paper. Fig. 8 shows all captured spirals for one bending direction for the three materials, as well as the measured curvatures along the spiral profiles. As a reference for the fitting results, the following table shows density ( $\rho$ , in  $kg/m^2$ ), stiffness ( $k_1 + k_2 \epsilon$ , in  $(N \cdot m) \times 10^{-7}$ ), maximum stress ( $a + b \epsilon$ , in  $N \times 10^{-4}$ ), and time constant ( $\tau$ , in  $1/m$ ), for the warp direction on the three samples.

	$\rho$	$k_1$	$k_2$	$a$	$b$	$\tau$
felt	0.208	145.3	0.15	5.12	0.15	29.9
doublecloth	0.255	62.19	0.07	12.84	0.05	7.67
paper	0.075	479.7	0.47	0.04	0.64	10.2

Fig. 10 shows photographs of representative spirals for the three materials (for 4mm, 7.5mm, and 23mm initial radii). Fig. 9 shows the estimated hysteresis curves with unload paths for the three initial radii, and the torque optimization residual at the sample points. Notice that the residual is overall low compared to the measured gravity-plus-elasticity torque.

Fig. 10 also shows final snapshots of unrolling simulations executed with the estimated parameters. The accompanying video compares the simulations to real-world footage of unrolling experiments. The simulation results demonstrate characteristic features of both final spiral profiles and dynamic unrolling, with good qualitative matches to real-world results, and strong differences across materials. Improving accuracy would require not only more accurate internal friction, but also accurate damping and contact friction.

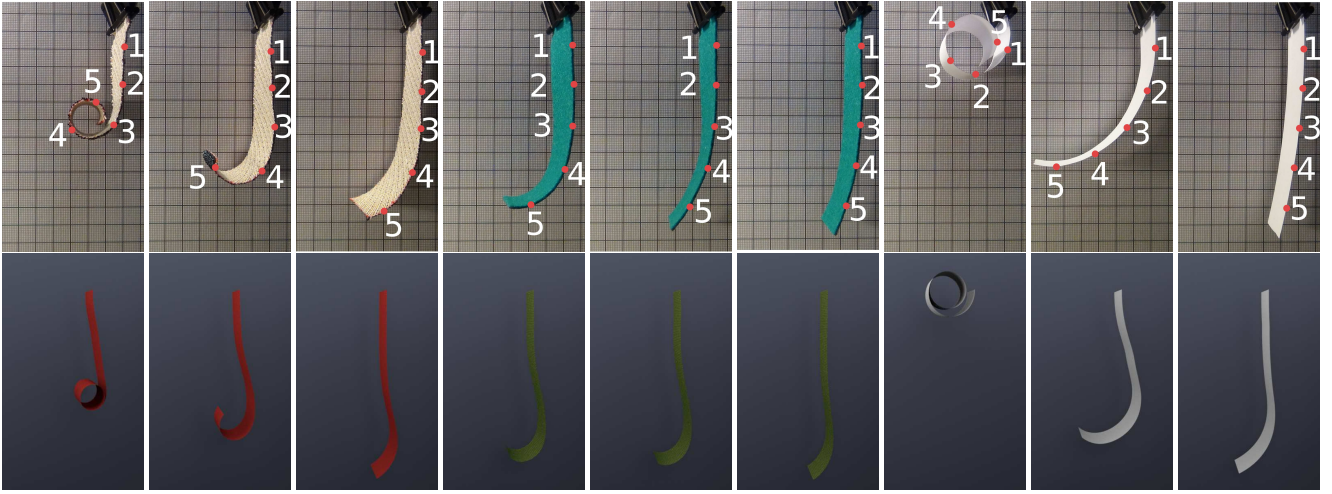


**Figure 10:** Comparison of captured and simulated unrolling spirals for initial radii of 4mm, 7.5mm, and 23mm for doublecloth (left), felt (center), and paper (right). The dots and numbers indicate samples for estimation residual evaluation in Fig. 9.

## 5 Dynamic Simulation of Internal Friction

Modeling internal friction in the context of dynamic simulation requires answering several challenges. First, we seek an easy integration into existing cloth simulators, which implies that Dahl’s model should be formulated as an explicit force expression (and possibly its derivatives w.r.t. positions and velocities) to be evaluated every time step. However, Dahl’s model is expressed in differential form, hence a straightforward integration in dynamic simulators would require the inclusion of new state variables. Instead, we propose an algorithm that allows handling Dahl’s friction force just as any other force expression.

The second challenge concerns stability and performance of the simulation. The stiffness of Dahl’s model is given directly by its differential expression in Eq. (2). At zero strain, the maximum stiffness is  $\frac{2a}{\tau}$  (for  $\sigma = -\sigma_{\max}$ ). Based on our estimated values, the effective stiffness of Dahl’s friction can be in the order of 100 times larger than the elastic stiffness. Given this high stiffness, it is crucial to design a simulation algorithm for implicit integration, stable under reasonably large time steps.

To formulate an explicit expression of friction force, we start by expressing the time derivative of the friction stress. Applying the chain rule to Eq. (2),

$$\dot{\sigma} = \frac{d\sigma}{d\epsilon} \dot{\epsilon} = \frac{1}{\tau} (\sigma_{\max}(\epsilon) - s\sigma) \dot{\epsilon}. \quad (8)$$

Dahl’s model becomes an ODE, and the friction stress becomes part of the dynamic state of the cloth (together with positions and velocities). This growth of the state would complicate the inclusion of Dahl’s model in existing cloth simulators, with the need of major changes to numerical solvers for implicit integration.

However, we note that the friction stress due to a strain element is a function of only the strain, strain rate, and stress at the element itself. Then, with backward Euler integration and a simple local linearization of Eq. (8) w.r.t  $\epsilon$ ,  $\dot{\epsilon}$ , and  $\sigma$  at every time step, we turn the (dynamic) friction stress into a linear function dependent only on the strain rate:

$$\sigma = \sigma_0 + \Delta t \frac{a + b\epsilon_0 - s_0\sigma_0 + \Delta t b \dot{\epsilon}_0}{\tau + \Delta t s_0 \dot{\epsilon}_0} \dot{\epsilon}. \quad (9)$$

This function can be trivially evaluated just like any other force in the dynamics simulator, and its derivatives can be added to the

system Jacobian for implicit integration. All values with a subindex 0 indicate values evaluated at the beginning of the time step (i.e., at the point of linearization), and  $\Delta t$  is the time step.

The simulation algorithm for implicit integration with our internal friction model is:

1. Evaluate friction stress values at the beginning of the time step using the analytic expression in Eq. (3), with the values from the previous time step as initial conditions.
2. Evaluate the Jacobians of friction stress according to Eq. (9).
3. Evaluate other forces and their Jacobians.
4. Formulate a linear system based on the implicit integration method of choice, and solve for cloth positions and velocities.

The algorithm above assumes one Newton iteration for (linearized) implicit integration, but it can be extended to iterate until convergence. In this case, friction stress values may only be re-evaluated once the solution has converged, not on every iteration of the solver, to ensure that friction follows the correct path. The same principle is applied as part of contact handling: friction stress values may only be re-evaluated once collisions are resolved, not inside iterative contact solvers.

As discussed in the next section, in our examples we found no difference between the time step requirements with and without friction, as the main source of time step restrictions turned out to be handling of self-collisions. Without collision handling, we found that implicit integration of friction forces enables stable integration under large time steps (e.g., more than 15ms for the cylinder demos in Figs. 11-13).

## 6 Results

We have executed multiple simulation tests to evaluate the effect and performance of our internal friction model and simulation algorithm on cloth simulations. From the purely mechanical point of view, our measurements indicate that the lack of friction may cause force and/or position deviations of up to 50%. From a visual point of view, force errors are not directly relevant, but we have observed that internal friction affects in multiple ways the formation and dynamics of folds and wrinkles. Next, we start with a discussion of friction effects on simple examples, where those effects are easier



**Figure 11:** Persistent wrinkles for cotton (left) and doublecloth (right) after a twist is quickly undone. The first and third images show wrinkles with friction and damping. The second and fourth images show more subtle wrinkles without damping, because vibrations partially eliminate the persistent deformations.

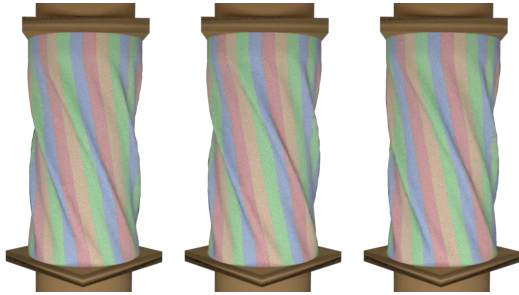


**Figure 12:** Wrinkles on a cotton cylinder with stretch friction after 1, 2, and 3 twist cycles. With internal friction, wrinkles are qualitatively similar, but arise at different locations after each twist cycle. Without friction (shown in the video), wrinkles are repetitive.

to isolate. Then, we discuss friction effects and the performance of our model and algorithm on larger character animation examples. We have used the damping model by Baraff and Witkin [1998], with damping values between one tenth and one hundredth of the stiffness at unit strain.

**Persistent Deformations** As already discussed, bending friction is the key phenomenon that produces the distinct persistent spiral profiles shown in Fig. 10. In these benchmarks, the overall dynamic behavior is influenced by other factors such as damping and contact friction, but the explosiveness of the unrolling effect is highly determined by internal forces, both elastic and friction forces. Paper turned out to be the most challenging material to simulate in these examples, due to the fast motion and high stiffness-to-mass ratio. We executed the simulations with a time step of 0.25ms to resolve all self-collisions robustly.

We have also compared the formation of persistent deformations under different settings. Fig. 11 shows examples of a sheet of cloth tightly wrapped around a cylinder. The cloth undergoes a quick twist-untwist motion, which is similar to the motion of a sleeve when the wrist is rotated. The figure compares persistent deformations for cotton (using stretch friction only) and doublecloth (using bending friction only) with and without damping. Without damping, cloth exhibits vibrations when the twist motion ends, and as a result the persistent wrinkles are more subtle.

**Preferred Folds and Wrinkles** The benchmark shown in Fig. 1 is a clear example of the influence of internal friction on the existence of ‘preferred wrinkles’. A localized stretch deformation is applied to a piece of cloth, and the persistent deformation induces



**Figure 13:** Images of a cylinder of cotton once a twist motion is undone, without friction (left) and with friction (right). The first (resp. third) and second (resp. fourth) snapshots are 0.5sec apart. Without friction, wrinkles slide along the surface, while friction stops them more rapidly.

a preferred wrinkle when the cloth is compressed in the transversal direction. As shown in the video, with our internal friction model we achieve a behavior that closely matches the real world. Under different angles and directions of compression, the simulation with internal friction tends to produce similar wrinkles, whereas the frictionless simulation exhibits highly varying wrinkles.

**History-Dependent Folds** Internal forces with friction are not conservative, hence the deformation under given boundary conditions is not defined as a simple energy minimum in the space of cloth configurations. In practice, this observation implies that the folds and wrinkles of cloth may differ largely for the same boundary conditions, and depend on history, i.e., the path traveled to reach those boundary conditions. Fig. 12 shows cloth wrinkles on a cylinder of cotton (with stretch friction) after several cycles of twist motions. With purely elastic deformations (not shown), the wrinkles are repetitive, but with the addition of friction wrinkles are different after each twist cycle.

**Settling of Wrinkles** Friction resists motion, and sometimes it even stops it. In connection with this property, internal friction of cloth helps wrinkles settle faster when external motion stops. Fig. 13 compares wrinkles on a cylinder of cloth when a twist motion is undone, with and without friction. It shows snapshots 0.5sec apart, once the external motion is over. Without friction, wrinkles slide longer, whereas friction stops them more rapidly.

**Character Clothing** We have simulated two examples of characters wearing clothing. The pants shown in Fig. 14 are represented using a 20K triangle mesh, and are attached to the character at the waist and ankles. The character shown in Fig. 15 wears pants represented by an 17K triangle mesh, and again attached at the waist and ankles. The T-shirt is represented by a 12K triangle mesh and is not attached. In both examples, we used for the cloth model parameters estimated from the cotton sample described in Section 4.

The pants in Fig. 14 show clear persistent deformations induced by friction. When the character lifts the knee, the fabric around the knee is strongly stretched. The persistent local stretch that remains when the knee is lowered produces a more irregular surface than the frictionless case. The visual appearance of this persistent deformation is different from thin localized wrinkles typically induced by plastic deformations.

The shirt of the character in Fig. 15 shows more stable folds and wrinkles with friction. The images highlight folds on the left side of the character’s chest. Without friction, the folds disappear half-



**Figure 14:** Simulation of cotton pants with stretch friction (right) and without (left). When the character lifts the knee, the fabric is stretched, and internal friction produces persistent deformations in the stretched areas. They are visible particularly between the knee and ankle on the rightmost image.

way through a jumping jack motion. The accompanying video also shows folds and wrinkles that settle faster with friction when the character performs squats.

We used a time step of 1ms for the simulation in Fig. 14, and 0.5ms for the simulation in Fig. 15, both for the friction and frictionless cases. In all cases, the time step restrictions were imposed by robust constraint-based handling of collisions and self-collisions. Despite having a numerical stiffness up to 100 times larger than the frictionless case, our implicit integration algorithm provides stable simulation for the internal friction model. The simulations were computationally expensive, mainly due to the implicit integration of nonlinear elasticity and friction coupled with LCP-type contact handling. The character simulation took an average of 6sec per time step on a single core of a 2.67 GHz Intel Core i7 920 CPU with 12 GB RAM.

## 7 Discussion and Future Work

In this work, we have presented a model of internal friction that captures the hysteresis of force-deformation in cloth, whose parameters can be estimated through simple procedures, and can be easily integrated into existing cloth simulation frameworks. It constitutes a step forward toward higher realism in cloth animation, but it also opens up several avenues of further work.

Our current friction model and estimation procedures present several limitations. The bending friction estimation procedure is not sufficiently sensitive for fabrics with very low bending-stiffness-to-density ratio, because the fabric’s weight clearly dominates elastic and friction forces together. We anticipate, however, that an estimation procedure based on anchor deformations might be designed for such fabrics too. Shear hysteresis appears to be at least as large as stretch or bending hysteresis, and estimation of shear friction parameters would require the design of a suitable estimation procedure. The challenge stems from the difficulty to impose controlled shear deformations that can be employed as anchor deformations in our estimation procedures.

Our friction model is conveniently expressed as a scalar stress dependent on an individual scalar strain, and this formulation cannot capture potential cross-modal effects. However, such potential cross-modal effects are hardly understood to date. In general, with the availability of good internal friction models, it would be conve-

nient to revisit the existing methods for the estimation of elasticity, and address the joint estimation of elasticity and friction. Based on our experiments, this need has become particularly evident for bending estimation on light materials. Following with a further understanding of internal friction, it would also be necessary to evaluate the effect of external factors such as moist on friction forces.

## Acknowledgements

We wish to thank Alvaro Perez and Gabriel Cirio for their help with the video, and the reviewers for their helpful and constructive feedback. This work was supported in part by the European Research Council (ERC-2011-StG-280135 Animetrics) and the Spanish Ministry of Economy (TIN2012-35840). We would like to thank Victor Zordan and the Berkeley Garment Library [de Joya et al. ] for the mannequin in the pants demo. All images were rendered using Mitsuba<sup>1</sup>.

## References

- BARAFF, D., AND WITKIN, A. 1998. Large steps in cloth simulation. In *Proc. of ACM SIGGRAPH*, 43–54.
- BARAFF, D. 1991. Coping with friction for non-penetrating rigid body simulation. In *Computer Graphics (Proceedings of SIGGRAPH 91)*, 31–40.
- BERGOU, M., MATHUR, S., WARDETZKY, M., AND GRINSPUN, E. 2007. Tracks: Toward directable thin shells. *ACM Transactions on Graphics* 26, 3 (July), 50:1–50:10.
- BLIMAN, P. A., AND SORINE, M. 1991. Friction modelling by hysteresis operators. application to dahl, stiction and stribeck effects. *Proc. Models of Hysteresis*.
- BREEN, D., HOUSE, D., AND WOZNY, M. 1994. Predicting the drape of woven cloth using interacting particles. In *Proc. of ACM SIGGRAPH*, 365–372.
- BRIDSON, R., FEDKIW, R., AND ANDERSON, J. 2002. Robust treatment of collisions, contact and friction for cloth animation. In *Proc. of ACM SIGGRAPH*, 594–603.

<sup>1</sup><http://www.mitsuba-renderer.org>



**Figure 15:** A character performing jumping jacks. Cloth is simulated without friction on the left, and with friction on the right. Internal friction produces more stable wrinkles and folds. This effect is particularly visible in the folds on the left side of the character's chest. Without friction, these folds disappear half-way through the motion, but they remain under friction.

- CHEN, Z., FENG, R., AND WANG, H. 2013. Modeling friction and air effects between cloth and deformable bodies. *ACM Transactions on Graphics* 32, 4.
- CHOI, K.-J., AND KO, H.-S. 2002. Stable but responsive cloth. In *Proc. of ACM SIGGRAPH*, 604–611.
- CLAPP, T. G., PENG, H., GHOSH, T. K., AND EISCHEN, J. W. 1990. Indirect measurement of the moment-curvature relationship for fabrics. *Textile Research J.* 60, 9.
- CULPIN, M. F. 1979. The shearing of fabrics: A novel approach. *J. Textile Institute* 70, 3, 81–88.
- DAHL, P. R. 1968. A solid friction model. Tech. rep., The Aerospace Corporation.
- DE JOYA, J. M., NARAIN, R., O'BRIEN, J., SAMII, A., AND ZORDAN, V. Berkeley garment library. <http://graphics.berkeley.edu/resources/GarmentLibrary/>.
- EBERHARDT, B., WEBER, A., AND STRASSER, W. 1996. A fast, flexible, particle-system model for cloth draping. *IEEE Computer Graphics and Applications* 16, 5, 52–59.
- ETZMUSS, O., KECKEISEN, M., AND STRASSER, W. 2003. A Fast Finite Element Solution for Cloth Modelling. In *Proc. Pacific Graphics*, 244–251.
- GRINSPUN, E., HIRANI, A., DESBRUN, M., AND SCHRÖDER, P. 2003. Discrete shells. In *Proc. ACM SIGGRAPH/Eurographics SCA*, 62–67.
- KALDOR, J. M., JAMES, D. L., AND MARSCHNER, S. 2008. Simulating knitted cloth at the yarn level. *ACM Trans. Graph. (Proc. SIGGRAPH)* 27, 3, 65:1–65:9.
- KAWABATA, S. 1980. The standardization and analysis of hand evaluation. *Textile Machinery Soc. Japan*.
- KIM, B.-C., OH, S., AND WOHN, K. 2011. Persistent wrinkles and folds of clothes. *International Journal of Virtual Reality* 10, 1, 61–66.
- LAHEY, T. J. 2002. *Modeling Hysteresis in the Bending of Fabrics*. Master's thesis, University of Waterloo.
- MIGUEL, E., BRADLEY, D., THOMASZEWSKI, B., BICKEL, B., MATUSIK, W., OTADUY, M. A., AND MARSCHNER, S. 2012. Data-driven estimation of cloth simulation models. *Computer Graphics Forum (Proc. of Eurographics)* 31, 2.
- MÜLLER, M., AND GROSS, M. H. 2004. Interactive virtual materials. In *Graphics Interface 2004*, 239–246.
- NARAIN, R., PFAFF, T., AND O'BRIEN, J. F. 2013. Folding and crumpling adaptive sheets. *ACM Transactions on Graphics* 32, 4.
- NGO-NGOC, C., AND BOIVIN, S. 2004. Nonlinear cloth simulation. Tech. rep., INRIA.
- OGDEN, R. W. 1997. *Non-Linear Elastic Deformations*. Courier Dover Publications.
- PADTHE, A., DRINCIC, B., OH, J., RIZOS, D., FASSOIS, S., AND BERNSTEIN, D. 2008. Duhem modeling of friction-induced hysteresis. *Control Systems, IEEE* 28, 5, 90–107.
- SHERBURN, M. 2007. *Geometric and Mechanical Modelling of Textiles*. PhD thesis, University of Nottingham.
- TERZOPOULOS, D., PLATT, J., BARR, A., AND FLEISCHER, K. 1987. Elastically deformable models. In *Proc. of ACM SIGGRAPH*, 205–214.
- THOMASZEWSKI, B., PABST, S., AND STRASSER, W. 2009. Continuum-based strain limiting. *Computer Graphics Forum (Proc. of Eurographics)* 28, 569–576.
- VOLINO, P., COURCHESNE, M., AND MAGNENAT-THALMANN, N. 1995. Versatile and efficient techniques for simulating cloth and other deformable objects. In *Proc. of ACM SIGGRAPH*, 137–144.
- VOLINO, P., MAGNENAT-THALMANN, N., AND FAURE, F. 2009. A simple approach to nonlinear tensile stiffness for accurate cloth simulation. *ACM Trans. Graph.* 28, 4.
- WANG, H., RAMAMOORTHY, R., AND O'BRIEN, J. 2011. Data-driven elastic models for cloth: Modeling and measurement. *ACM Trans. Graph. (Proc. SIGGRAPH)* 30, 4, 71.
- WILLIAMS, R. W. 2010. *Measuring and Modeling the anisotropic, nonlinear and hysteretic behavior of wooven fabrics*. PhD thesis, University of Iowa.
- ZHU, Y., AND BRIDSON, R. 2005. Animating sand as a fluid. *ACM Transactions on Graphics* 24, 3 (Aug.), 965–972.